ISSN 0031-918X, Physics of Metals and Metallography, 2021, Vol. 122, No. 6, pp. 621–627. © Pleiades Publishing, Ltd., 2021.
Russian Text © The Author(s), 2021, published in Fizika Metallov i Metallovedenie, 2021, Vol. 122, No. 6, pp. 665–672.

STRENGTH AND PLASTICITY

Effect of Deformation-Thermal Processing on the Microstructure and Mechanical Properties of Low-Carbon Structural Steel

S. N. Sergeev[a], *, I. M. Safarov[a], A. P. Zhilyaev[a], R. M. Galeev[a], S. V. Gladkovskii[b], and D. A. Dvoinikov[b]

[a] *Institute for Problems of Metal Superplasticity, Russian Academy of Sciences, Ufa, 450001 Russia*
[b] *Institute of Engineering Science, Ural Branch, Russian Academy of Sciences, Ekaterinburg, 620049 Russia*
**e-mail: nikocem17@gmail.com*

Received November 25, 2020; revised February 4, 2021; accepted February 12, 2021

Abstract—An ultrafine-grained (UFG) structure of equiaxed and fiber types in the low-carbon structural steel 05G2MFBT (Fe–2Mn–Mo–V–Nb–Ti) has been formed with various techniques of deformation-heat treatment. This steel with a UFG structure has been found to exhibit higher strength properties. Different deformation techniques have been shown to produce either a fibrous or an equiaxed UFG structure with carbide particles of a wide range of sizes. The brittle fracture resistance of the fibrous UFG steel has been found to be higher than that of the fine-grained steel after controlled rolling and subsequent accelerated cooling. Standard bending-impact tests have shown that the steel with a fibrous UFG structure is characterized by higher impact strength characteristics and a lower ductile–brittle transition temperature.

Keywords: low-carbon steel, impact strength, ultrafine-grained structure

DOI: 10.1134/S0031918X21060090

INTRODUCTION

The development of promising structural materials and hardening conditions that ensure high reliability and a long service life of the parts, units, and elements of important engineering structures designed for operation under static and dynamic loads in a wide temperature range is an actual task of modern materials science. These materials include low-alloyed low-carbon steels, which are widely used in industry at present, because they make it possible to achieve the required mechanical properties while maintaining good manufacturability and a relatively low production cost [1, 2]. However, the significant disadvantages of these steels include an insufficiently high strength and low brittle fracture resistance at low ambient temperatures, which is typical of BCC metals [3, 4]. One way to increase the strength properties and decrease the cold-brittleness threshold temperature of low-carbon structural steels is to form ultrafine-grained (UFG) and nanocrystalline (NC) structures in them with severe deformation techniques, such as ECA pressing [5] and multiaxis isothermal forging (MIF) [6].

Another way to increase the impact strength at room and low temperatures is to form a layered-fibrous structure in ferritic and ferrite–pearlitic structural steels of different compositions via hot rolling [7, 8] or warm rolling at the temperatures of tempering of preliminarily quenched steels [9]. A recent deformation–heat treatment regime was called "tempforming" [10]. Some Russian and foreign works have shown that a fibrous UFG structure in low-carbon steels can both increase the impact strength with shifting the cold-brittle threshold temperature towards lower temperatures [11, 12] and cause an anomalous maximum in the temperature dependence of the absorbed impact energy [13]. In the latter case, the absorbed impact energy of steels increases in the temperature range of ductile–brittle transition due to the effect of "delamination toughening" [14]. Although the influence of a fibrous UFG structure on the mechanical properties of low-carbon steels has been examined in detail in the scientific literature, the anomalous increase in the impact strength characteristics with a decrease in the test temperature remains unstudied and requires further detailed analysis. We should note that the influence of warm rolling on the structure formation, tensile mechanical properties, and temperature dependences of the impact toughness of low-carbon steels (C ≈ 0.1–0.15%) is still poorly studied in contrast to those of medium-carbon steels (C ≈ 0.4–0.6%) [14, 15]. Therefore, the goal of this work is to analyze the effect of severe deformation via MIF and warm rolling at 550°C on the evolution of the structure, texture, mechanical tensile properties, and temperature dependence of the impact strength properties of the low-carbon structural steel 05G2MFBT.

Table 1. Chemical composition of 05G2MFBT steel (wt %)

Fe	C	Mn	Si	V	Nb	P	S	Mo	Ti
Balance	0.054	1.61	0.26	0.025	0.059	0.009	0.0012	0.192	0.023

EXPERIMENTAL

The 05G2MFBT steel was subjected to controlled rolling and accelerated cooling to obtain samples 20 × 20 × 100 mm in size. Table 1 lists the chemical composition of the 05G2MFBT steel. To form the UFG fibrous and the equiaxed structure, we also carried out deformation via warm rolling and MIF. The rolling was performed at 550°C with an MKU-280 rolling mill. The steel workpieces were rolled between four calibrating, rectangular-sectioned rolls in several passes to form bars 10 mm × 10 mm in cross section at a relative reduction of $\psi = 10–15\%$ for one pass. The total accumulated true strain was estimated with the formula: $e = \Sigma\ln(F_{i-1}/F_i)$, where F_{i-1} and F_i are the initial and final areas of the cross section of the bar at each rolling stage. The accumulated true strain after rolling was $e = 2.7$.

Deformation by means of MIF was carried out on a PA 2638 hydraulic press at 550°C in the strain rate range $10^{-3}–10^{-2}$ s^{-1} to form a relatively equiaxed structure. The total accumulated true strain was $e = 10.5$.

The steel structure was examined via transmission electron microscopy (TEM) and scanning electron microscopy (SEM). The fine structure of the steel was examined with a JEOL JEM 2000EX transmission electron microscope. The microstructural parameters were analyzed automatically by means of backscattered electron diffraction pattern (EBSD) analysis with a Tescan Mira 3LMH scanning electron microscope. The calculation was carried out with CHANNEL 5 software at a scanning step from 50 to 200 nm. The fraction of diffraction patterns identified from the six Kikuchi lines was at least 80% of the total number of measured points. The criterion for the division of the boundaries into low-angle (LABs) and high-angle (HABs) boundaries was a 15° misorientation. Boundaries with misorientation of less than 2° were excluded from the analysis due to the insufficient accuracy of their determination [16].

Statistical tensile tests of flat samples of type I were carried out according to State Standard GOST 1497–84 on an INSTRON-1185 universal dynamometer at room temperature at a strain rate of $\dot{\varepsilon} = 10^{-3}$ s^{-1}.

Bending-impact tests of the standard samples of type 11 with a V-notch 2 mm deep oriented by the "crack-arrester" type [17] was conducted according to GOST 9454–78 with a Tinius Olsen IT542M impact pendulum in a temperature range of 20 to –196°C. Impact-loading diagrams were built in load–displacement coordinates in a temperature range of 20°C to –196°C with pendulum software. The results of the processing of load diagrams according to the recommendations of State Standard GOST 22848–77 were used to divide the total impact energy (A) into components, such as the work for crack nucleation (A_n) and crack initiation (A_p). The index of dynamic crack resistance (J_{id}) was calculated with the technique described in [18]:

$$J_{id} = 2A_n/B(W-a),$$

where B is the sample width, W is the sample height, and a is the length of the stress concentrator (notch). The mechanical properties were averaged according to the test results of at least three identical samples, and the spread did not exceed ±2.5%.

Fractographic analysis of the fracture surface of the samples was performed on a Tescan Vega 3SBH scanning electron microscope.

RESULTS AND DISCUSSION

The structure of the 05G2MFBT steel after controlled rolling and subsequent accelerated cooling matches completely with the bainite structure described in [19] with an average grain size of 5–10 μm.

Warm rolling resulted in a UFG structure with severely elongated grains 600 ± 150 nm in mean cross-sectional size. The fiber length in the longitudinal section was 20–30 μm. Carbide particles are distributed along the fiber boundaries (Fig. 1b). In contrast to rolling, MIF results in an equiaxed structure with an average grain size of 800 ± 150 nm in all sections. The grains contain an increased defect density. The grain boundaries are mostly typical of a deformed structure; that is, they are wide and twisted, contain an increased defect density, and are highly nonequilibrial. There are also smooth and thin equilibrium boundaries, which are typical of recrystallized grains.

Additional EBSD analysis allowed us to estimate the processes that took place under different conditions of deformation–heat treatment.

Figure 2 shows the EBSD maps of the 05G2MFBT steel microstructure after three different deformation–heat treatment regimes. The changes that occurred in the controlled-rolled structure due to subsequent warm rolling or MIF can be seen.

The results shown in Table 2 showed that the fraction of LABs in the cross and longitudinal sections after controlled rolling is approximately the same and is 26 and 28%, respectively. The fraction of special boundaries does not exceed 5% in both sections.

Warm rolling at 550°C resulted in a significant increase in the fraction of LABs in the 05G2MFBT steel to 48% in the cross section and 36% in the longi-

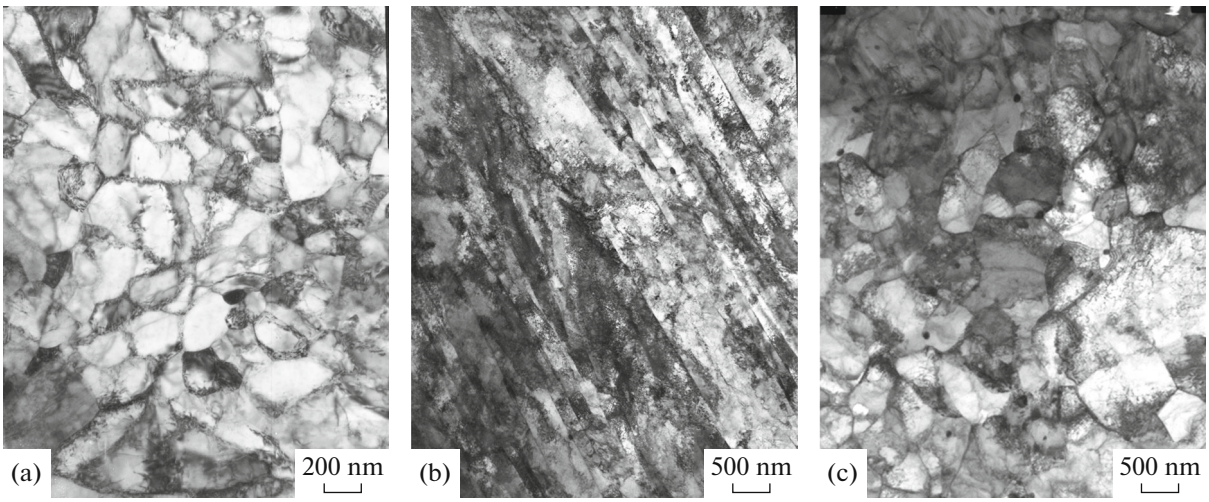

Fig. 1. Microstructure of 05G2MFBT steel after (a) warm rolling in the cross section, (b) warm rolling in the longitudinal section, and (c) MIF.

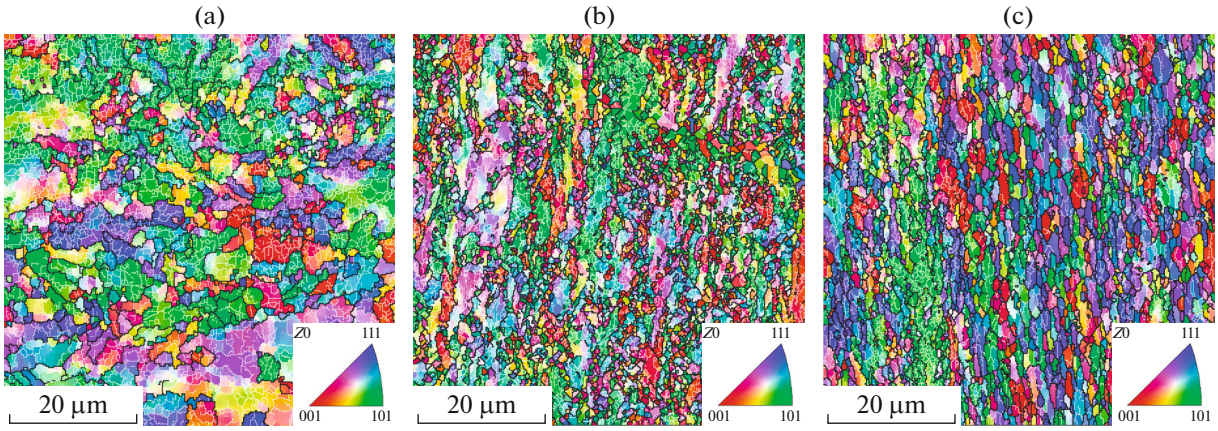

Fig. 2. Orienting EBSD maps of the 05G2MFBT steel microstructure in the cross section after (a) controlled rolling and subsequent accelerated cooling, (b) warm rolling, and (c) MIF. Schematic of grain (black) and subgrain (white) boundaries.

tudinal section. The fraction of special boundaries changed insignificantly and increased to 8% in both sections. The significant differences in the fraction of LABs in the longitudinal and cross sections indicate nonequilibrial deformation during warm rolling and further structure refinement, including that due to the

Table 2. Fractions of low-angle, high-angle, and special boundaries (all types), and the average grain size in 05G2MFBT steel after various treatment conditions

Treatment conditions	Fraction of LABs, %	Fraction of HABs, %	Fraction of special boundaries, %	Average grain/subgrain size, μm
After controlled rolling (cross section)	26	71	4	5.1
After controlled rolling (longitudinal section)	28	68	5	4.1
After warm rolling at 550°C (cross section)	48	45	7	0.6
After warm rolling at 550°C (longitudinal section)	36	57	8	–
After MIF at 550°C (cross section)	45	48	7	0.9
After MIF at 550°C (longitudinal section)	34	57	9	0.8

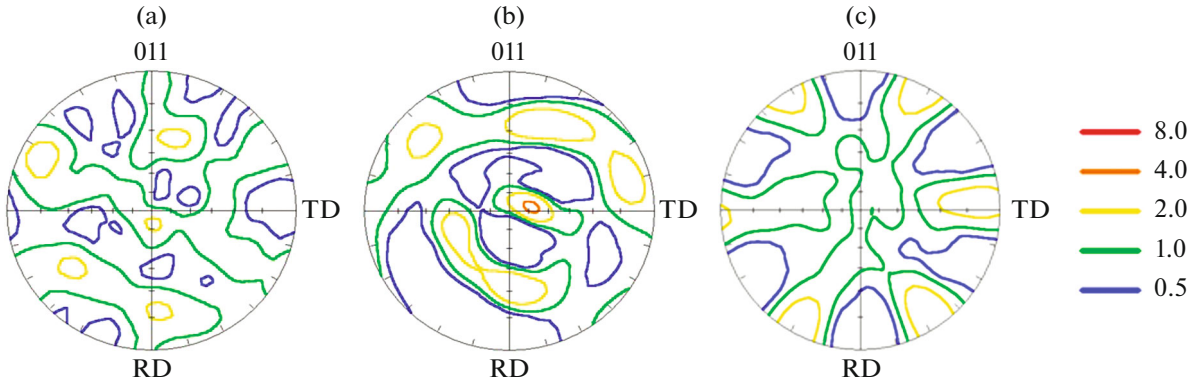

Fig. 3. Direct pole figures of 05G2MFBT steel samples in the cross section after (a) controlled rolling and subsequent accelerated cooling, (b) warm rolling, and (c) MIF.

formation of subgrains. Substructural hardening occurs more intensively in the cross section than in the longitudinal section, depending on the deformation scheme. A similar picture is observed in low-carbon steel after MIF; the only difference is that the fraction of LABs in the cross section is slightly lower than that after warm rolling, i.e., 45 and 48%, respectively.

Figure 2 shows that the steel microstructure after forging remains slightly elongated in a perpendicular direction to the last compression direction. Note that, unlike the transmission electron microscopy studies, EBSD analysis showed the presence of regions with both small grains and elongated coarse grains in the microstructure after warm rolling. The developed subgrain microstructure is observed inside the coarse grains. However, MIF produces a more homogeneous structure with fine, equiaxed grains against a background of elongated grains of the same orientation. These significant differences in the structure after different deformation schemes can be explained by the different character of the development of the dynamic recrystallization and polygonization processes.

Analysis of the pole figures (Fig. 3) showed that the two-component rolling texture of the initial state becomes sharper after warm rolling, and the axial component begins to dominate in it. The reason for this is that the used deformation scheme in the four-roll pass excludes the cross "flow" of the metal. Therefore, the deformation mainly proceeds along the rolling direction, leading to the preferential formation of the single-axis texture component. During MIF, the samples undergo compression with a change in the deformation axis during each pass. The initial rolling texture, in this case, is blurred, and the pole maxima rotate along the three axes of the sample.

The results of the mechanical tests presented in Table 3 indicate that the steel, even in the condition of delivery, has high strength properties and impact strength. The high properties are due to the bainitic structure that form in the material during controlled rolling and subsequent accelerated cooling [20, 21]. The average grain size in the bainitic structure is 5–10 μm. The grain and subgrain refinement makes the main contribution to the hardening.

Additional warm rolling increased $\sigma_{0.2}$ and σ_u from 700 to 1000 MPa in comparison with those in the initial state and decreased δ from 21 to 17%. The ultimate tensile strength and the yield strength in the longitudinal and cross sections do not exceed 10%. Conversely, the impact strength of the steel at room temperature increases after warm rolling and reaches $KCV^{20} > 3.38$ MJ/m^2 (not completely broken sample). Therefore, the formation of the fibrous UFG microstructure leads to a 1.5-fold increase in the strength characteristics of the steel due to grain, subgrain, and precipitation hardening.

The mixed grain-subgrain UFG structure formed by MIF, like the microstructure formed by warm rolling, increases the strength properties by 60%. The ratio $\sigma_{0.2}/\sigma_u = 0.97$ reaches its highest value, which indicates a decrease in the strain-hardening reserve of the steel and, accordingly, the resource of its plastic deformability. The relative elongation decreases from

Table 3. Mechanical properties of the 05G2MFBT low-carbon steel in the sample cross section

05G2MFBT	$\sigma_{0.2}$, MPa	σ_u, MPa	$\sigma_{0.2}/\sigma_u$	δ, %	KCV^{20}, MJ/m^2
After controlled rolling	612	685	0.89	21	3.15
After warm rolling	1017	1080	0.94	17	>3.38
After MIF	1056	1093	0.97	13	2.20

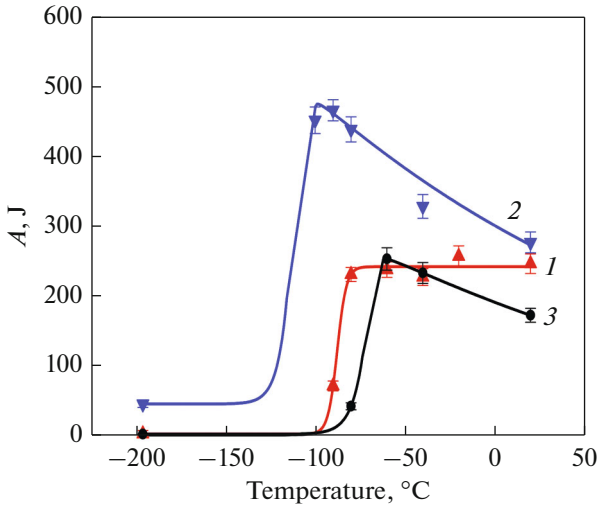

Fig. 4. Temperature dependence of the work of fracture of the 05G2MFBT steel: (*1*) after controlled rolling, (*2*) with a fibrous UFG structure, and (*3*) with an equiaxed UFG structure.

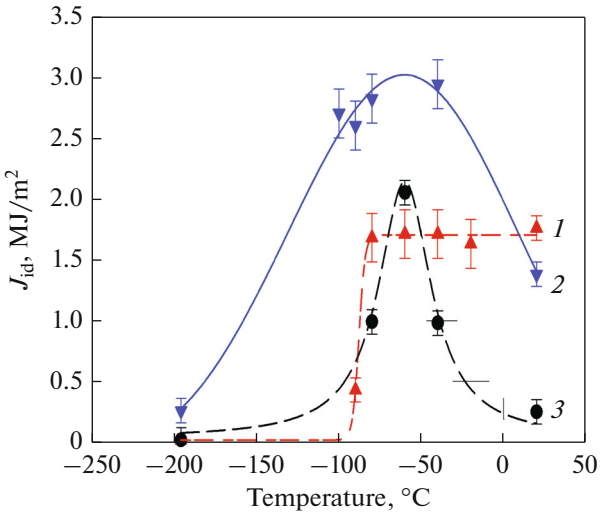

Fig. 5. Temperature dependence of the dynamic crack resistance of 05G2MFBT steel: (*1*) after controlled rolling, (*2*) with a fibrous UFG structure, and (*3*) with an equiaxed UFG structure.

21 (initial value) to 13% and the impact strength at room temperature decrease from 3.15 to 2.20 MJ/m^2.

Impact tests carried out in the range from room temperature to the boiling temperature of liquid nitrogen show that MIF reduces the impact work and dynamic cracking resistance (Figs. 4, 5) at temperatures of +20, −40, and −80°C due to severe strain-hardening of the steel and shifts the ductile–brittle transition temperature by about 20°C towards the region of higher temperatures.

The increase in structural imperfection during MIF decreases the ability of the steel to resist crack nucleation and propagation, which lowers the impact toughness properties at low temperatures. However, an abnormal increase in A and, especially, J_{id} is observed at a test temperature of −60°C (Figs. 4, 5). The highest anomalous increase in the impact strength of the 05G2MFBT steel after additional warm rolling is observed in a temperature range of −40 to −100°C (Figs. 4, 5).

We should note that the maximum impact work A after warm rolling is reached at −90°C, which corresponds to the transition temperature after the controlled initial rolling. A similar abnormal increase in impact strength is explained by the "delamination toughening" effect in low-carbon low-alloy steels [10], which is observed at transition temperatures. The high impact strength of the steel with a fibrous UFG structure formed via warm rolling remains the same at the temperature of liquid nitrogen, as compared to that of the steel after the controlled initial rolling and additional MIF (see Figs. 4 and 5).

In summary, we can note that crack nucleation and initiation during impact tests below −70°C occur via different mechanisms, depending on the type of the UFG structure in the 05G2MFBT steel treated in different ways. This is also confirmed via fractographic analysis of the fracture surface. For example, the loading diagrams clearly show the change in the stages of fracture processes of an impact sample at −80°C (Fig. 6).

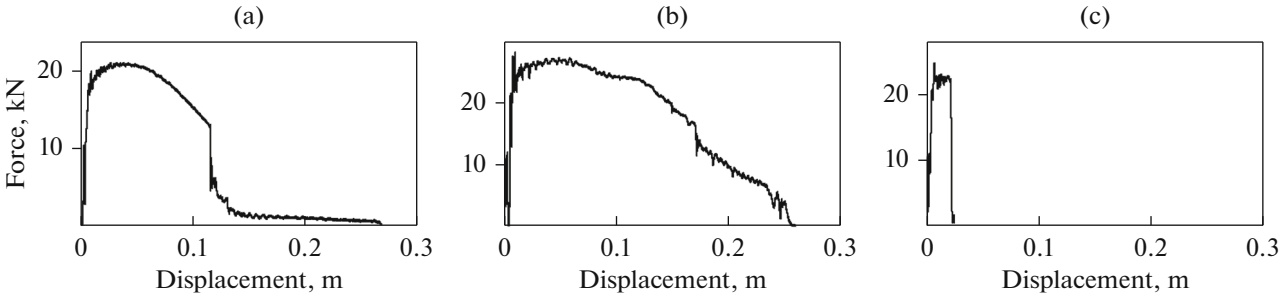

Fig. 6. Impact-loading diagrams of 05G2MFBT steel samples at −80°C after (a) controlled rolling and subsequent accelerated cooling, (b) warm rolling, and (c) MIF.

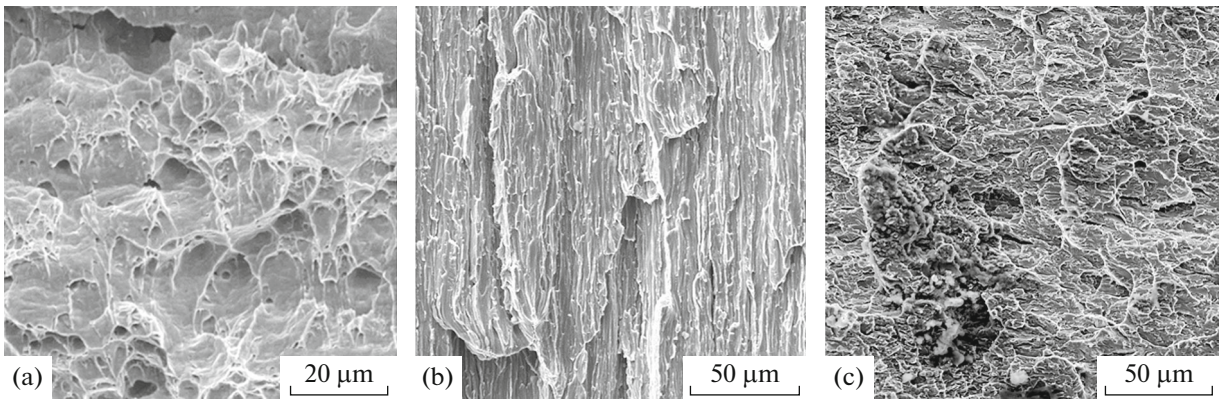

Fig. 7. Fracture-surface microstructure of the steel at a temperature of –80°C after (a) controlled rolling and subsequent accelerated cooling, (b) warm rolling, and (c) MIF.

The impact-loading diagram of initial steel samples at –80°C shows a brittle jump (Fig. 6a), which is accompanied by a decrease in the impact work and dynamic cracking resistance (Figs. 4, 5), while the ductile-dimple fracture microstructure (Fig. 7a) remains predominant. The highest impact-loading work (A = 420 J) and dynamic cracking resistance (J_{id} = 2.8 MJ/m^2) are achieved at a temperature of –80°C after warm rolling. These values agree well with the jump-like impact-loading diagram (Fig. 6b), which is typical of a fracture with delamination and the formation of a "terrace-type" fracture [13] (Fig. 7b). The loading diagram of the MIF-deformed steel samples at a temperature of –80°C is typical of brittle fracture (Fig. 6c). The quasi-cleavage relief of the crack surface prevails.

CONCLUSIONS

(1) The initial bainitic structure of 05G2MFBT steel obtained controlled rolling, which had an average grain size of 5–10 μm, was transferred after warm rolling into a fibrous UFG structure with an average grain cross section of 0.6 μm. After MIF, the steel structure became more equiaxed in longitudinal and cross sections and was characterized by an average grain size of 0.80 ± 0.15 μm. The largest fraction of HABs (68–71%) in all sections was achieved after controlled rolling, and the smallest fraction was achieved in the sample cross sections after warm rolling (45%) and MIF (48%).

(2) Warm rolling and MIF resulted in the formation of fibrous and equiaxed mixed UFG structures in the steel respectively. As a result, the strength properties increased by a factor of 1.6–1.7 to σ_u = 1080 MPa and σ_u = 1093 MPa, respectively, in comparison with the initial values, while the increased ductility (17 and 13%) and impact toughness at room temperature (3.38 and 2.20 MJ/m^2) remained the same.

(3) MIF reduced the impact-loading work and dynamic crack resistance of the steel at temperatures of +20, –40, and –80°C and also changed the ductile–brittle transition temperature. An abnormal increase in A and, especially, J_{id} is observed at a test temperature of –60°C after MIF.

(4) After warm rolling, an abnormal increase in the work of impact loading and dynamic crack resistance of the 05G2MFBT steel was observed in a test temperature range of –40 to –100°C. This growth can be explained by the formation of the fibrous UFG structure and the "delamination toughening" effect at transition temperatures.

(5) The relationship was revealed between the impact toughness of the steel at a temperature of –80°C, the type of shock-loading diagrams, and the microstructure of the fracture surface for the studied deformation treatment regimes. The "terrace"-type of fracture with delamination was observed in the samples after warm rolling.

ACKNOWLEDGMENTS

The scientific research was carried out at the Structural and Physical-Mechanical Studies of Materials Center of the Collaborative Use of the Institute for Problems of Metal Superplasticity of the Russian Academy of Sciences.

FUNDING

This work was performed within the state assignment of Institute for Problems of Metal Superplasticity of the Russian Academy of Sciences and Institute of Engineering Science, Ural Branch of the RAS for 2019–2021.

REFERENCES

1. O. A. Sofrygina, S. Yu. Zhukova, S. M. Bityukov, and I. Yu. Pyshmintsev, "Economical steels for the manufacture of high-strength oil pipe (according to the API

SPEC5CT standard)" Steel Transl. **40**, No. 7, 616–621 (2010).

2. L. M. Kleiner, K. A. Kobelev, S. K. Greben'kov, and D. M. Larinin, "A new class of structural steels in mechanical engineering," Metallurg. Mashinost., No. 5, 39–40 (2011).
3. V. A. Pavlov, *Physical Basics of Cold Deformation of BCC Metals* (Nauka, Moscow, 1978).
4. V. M. Chernov, B. K. Kardashev, and K. A. Moroz, "Cold brittleness and fracture of metals with various crystal lattices: dislocation mechanisms," Tech. Phys. **61**, 1015–1022 (2016).
5. R. Z. Valiev, G Klevtsov, N. A. Klevtsova, M. V. Fasenyuk, M. R. Kashapov, A. G. Raab, M. V. Karavaeva, and A Ganeev, "The influence of the modes of equal channel angular pressing and subsequent heating on the strength and the mechanism of failure of steel 10," Deformatsiya i Razrusheniya Materialov, No. 1, 21–25 (2013).
6. I. M. Safarov, A Korznikov, R. M. Galeev, S. N. Sergeev, S. V. Gladkovskii, and I. Yu. Pyshmintsev, "An anomaly of the temperature dependence of the impact strength of low-carbon steel with an ultrafine-grain structure," Dokl. Phys. **61**, 15–18 (2017).
7. V. M. Schastlivtsev, D. A. Mirzaev, I. L. Yakovleva, N. A. Tereshchenko, and T. I. Tabatchikova, "Effect of increasing impact toughness on the formation of a layered structure upon hot rolling of a ferritic steel," Dokl. Phys. **55**, 334–337 (2010).
8. D. A. Mirzaev, D Shaburov, I. L. Yakovleva, A Panov, L Elokhina, Factors responsible for increasing ductility of the ferritic steel 08Kh1ST1 In the course of repeated hot rolling," Phys. Met. Metallogr. **98**, No. 3, 317–325 (2004).
9. Dolzhenko A., Z. Yanushkevich, S. A. Nikulin, A. Belyakov, and R. Kaibyshev, "Impact toughness of an S700MC-type steel: Tempforming vs ausforming," Mater. Sci. Eng., A **723**, 259–268 (2018).
10. T. Inoue, F. Yin, Y. Kimura, K. Tsuzaki, and S. Ochial, "Delamination effect on impact properties of ultrafine-grained low-carbon steel processed by warm caliber rolling," Metall. Mater. Trans. A **41**, 341–355 (2010).
11. S. N. Sergeev, I. M. Safarov, A. V. Korznikov, R. M. Galeev, S Gladkovskii, and D. A. Dvoinikov, "Effect of warm rolling on the structure and mechanical properties of low carbon tube steel," Pis'ma Mater. **5**, No. 1, 51–54 (2015).
12. I. M. Safarov, A. V. Korznikov, R. M. Galeev, S. N. Sergeev, S. V. Gladkovskii, E. M. Borodin, and I. Yu. Pyshmintsev, "Strength and impact toughness of low-carbon steel with fibrous ultrafine-grained structure," Phys. Met. Metallogr. **115**, No. 3, 315–323 (2014).
13. Y. Kimura, T. Inoue, and K. Tsuzaki, "Tempforming in medium-carbon low-alloy steel," J. Alloys Compd. **577**, 538–542 (2013).
14. Y. Kimura, T. Inoue, F. Yin, and K. Tsuzaki, "Delamination toughening of ultrafine grain structure steels processed through tempforming at elevated temperatures," ISIJ Int. **50**, No. 1, 152–161 (2010).
15. Y. Kimura and T. Inoue, "Influence of warm tempforming on microstructure and mechanical properties in an ultrahigh-strength medium-carbon low-alloy steel, "Metall. Mater. Trans. A **44**, 560—576 (2013).
16. V. N. Danilenko, S. Yu. Mironov, A. N. Belyakov, and A. P. Zhilyaev, "Application of EBSD analysis in physical materials science (Review)," Zavod. Lab., Diagn. Mater. **78**, No. 2, 28–46 (2012).
17. J. D. Embury, N. J. Petch, A. E. Wraith, and E. S. Wright, "The fracture of mild steel laminates," Trans. Metall. Soc. AIME **239**, 114–118 (1967).
18. L. R. Botvina, *Failure: Kinetics, Mechanisms, General Relations* (Nauka, Moscow, 2008) [in Russian].
19. L. I. Efron, *Metal Science in "Large" Metallurgy. Pipe Steels* (Metallurgizdat, Moscow, 2012) [in Russian].
20. I. L. Yakovleva, N. A. Tereshchenko, and N Urtsev, "Observation of the martensitic-austenitic component in the structure of low-carbon low-alloy pipe steel," Phys. Met. Metallogr. **121**, No. 4, 352–358 (2020).
21. M. L. Lobanov, I. Yu. Pyshmintsev, V. N. Urtsev, S. V. Danilov, N Urtsev, and A. A. Redikul'tsev, "Texture inheritance in the ferrito-martensite structure of low-alloy steel after thermomechanical controlled processing," Phys. Met. Metallogr. **120**, No. 12, 1180–1186 (2019).

Translated by T. Gapontseva